CONF-9410314--4

UCRL-JC-118834
PREPRINT

Measurements of Large Scale-Length Plasmas Produced from Gas-Filled Targets

C. A. Back, R. L. Berger, K. Estabrook, B. H. Failor, W. W. Hsing, E. J. Hsieh, R. Hockaday, D. H. Kalantar, R. L. Kauffman, C. J. Keane, D. E. Klem, B. J. MacGowan, D. S. Montgomery, J. D. Moody, L. V. Powers, T. D. Shepard, G. F. Stone, L. J. Suter, and R. E. Turner

This paper was prepared for submittal to the
6th International Workshop on Radiative
Properties of Hot Dense Matter
Sarasota, Florida
October 31 - November 4, 1994

June 30, 1995

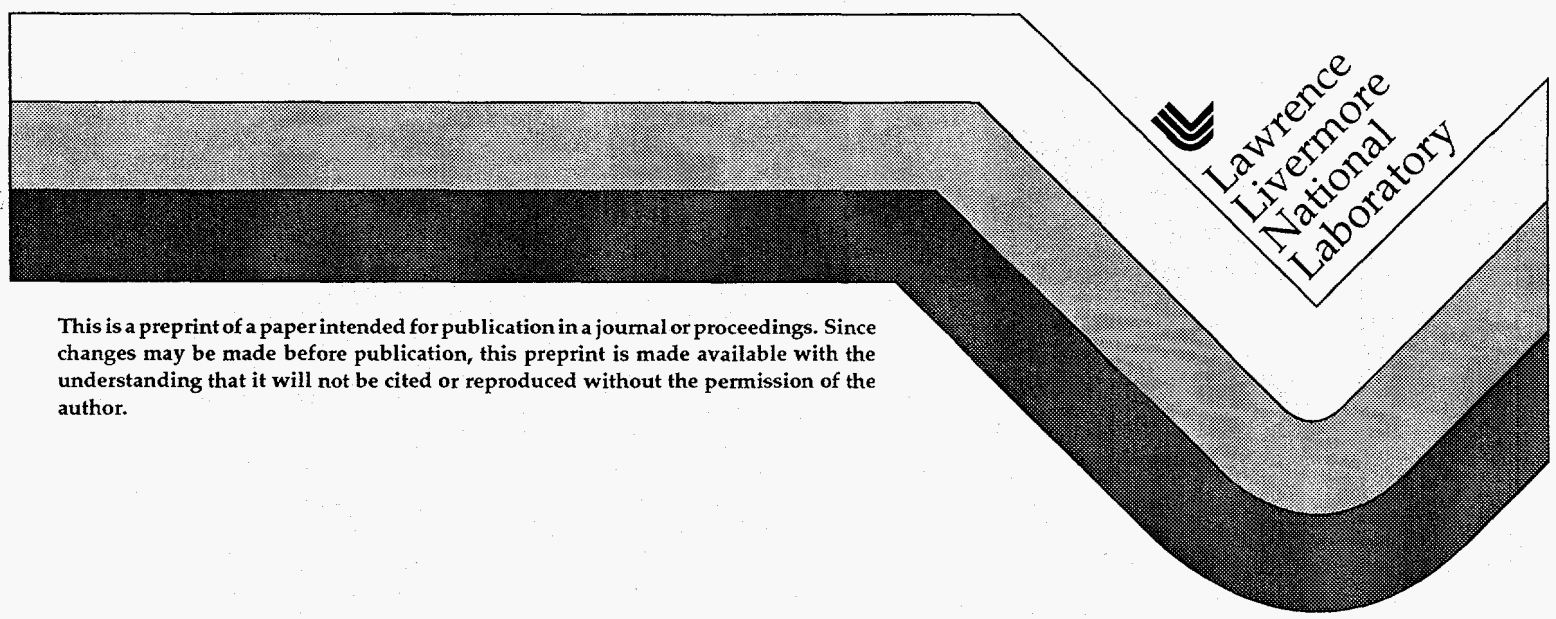

GH

DISCLAIMER

Measurements of Large Scale-Length Plasmas Produced from Gas-Filled Targets

C. A. Back, R. L. Berger, K. Estabrook, B. H. Failor†, W. W. Hsing†, E. J. Hsieh, R. Hockaday†, D. H. Kalantar, R. L. Kauffman, C. J. Keane, D. E. Klem, B. J. MacGowan, D. S. Montgomery, J. D. Moody, L. V. Powers, T. D. Shepard, G. F. Stone, L. J. Suter, and R. E. Turner

Lawrence Livermore National Laboratory,
P. O. Box 808, Livermore, CA 94551

†*Los Alamos National Laboratory,*
Loa Alamos, New Mexico 87545

Apart from their intrinsic interest, plasma physics processes are important because they affect the coupling of the laser energy into laser-irradiated targets. Recently, new gas-filled targets have been developed to create large mm-size plasmas for the study of stimulated Brillouin scattering (SBS) and stimulated Raman scattering (SRS). We present x-ray images and x-ray spectra to characterize these targets, which show that the plasmas are homogeneous, have electron densities of ~ 10^{21} cm^{-3}, and attain electron temperatures of ~3 keV. We also present SBS measurements to demonstrate how systematic studies of physical phenomena can be performed using these targets.

INTRODUCTION

Plasma interaction processes have been studied in numerous experiments that have revealed important laser-plasma interaction mechanisms in the absorption of laser light.[1] The laser-produced plasmas studied in the laboratory have usually involved disk or foil targets. Because of the hydrodynamic expansion of these targets, the resulting plasmas tend to have small density and velocity scale-lengths. In inertial confinement fusion (ICF), large mm-size plasmas are produced and the gradients in these targets may be very different. To study the absorption of laser light in these types of plasmas, a novel target design was developed. In this paper, we will present results on the characterization of plasmas produced from these targets as well as an example of the use of these plasmas as testbeds for the study of stimulated Brillouin scattering (SBS).

Large homogeneous plasmas are required for the study of parametric instabilities that are generated by lasers interacting with the plasmas of future inertial confinement fusion (ICF) targets. The plasma conditions can be characterized in terms of the velocity and density scale-lengths. The velocity scale-length is defined by the equation, $L_v = c_s (\partial v_z/\partial z)^{-1}$, where c_s is the ion sound speed and $(\partial v_z/\partial z)$ is the gradient of the flow velocity. Similarly, the density scale-length is given by, $L_n = n_e (\partial n_e/\partial z)^{-1}$, where n_e is the electron density and $(\partial n_e/\partial z)$ is the density gradient.

As an example of the scale-lengths of a common laser-produced plasmas, we note that in exploding foil targets, both of these scale-lengths are on the order of 500 to 600 μm.[2] On the other hand, for conditions relevant to future indirect drive ICF targets, the velocity and density scale-lengths are 6 mm and 2 mm,

respectively.[3] Partial confinement by the hohlraums helps to achieve these long density and velocity scale-lengths.

Calculations indicate that hohlraum plasmas created by 0.35 μm laser light for future ICF targets will have electron temperatures > 3 keV and electron densities of ~ 0.1 $n_{cr} = 10^{21}$ cm^{-3}, where n_{cr} is the critical density for laser light.

GAS-FILLED TARGETS AND EXPERIMENTAL CONFIGURATION

To produce plasmas having these scale-lengths required the development of a new type of target that is filled with gas confined by polyimide membranes. Polyimide is a commercial plastic which has a typical composition of $C_{14}H_6O_4N_2$. Schematics of two types of targets, a gas bag and a gas-filled hohlraum, are shown in figure 1. The gas bag is composed of a metal washer that has a thin polyimide membrane, initially 8500 Å thick, glued over each side. This target is then filled with a gas through tubes in the washer. The gas stretches each membrane to a nearly hemispherical shape, forming a near spherical gas bag that is approximately 2.75 mm in diameter. The gas-filled hohlraum consists of a 25 μm thick Au cylinder that is 2.5 mm long and 2.5 mm in diameter. Polyimide membranes 6000 Å thick cover 1875 μm diameter holes that allow the laser beams to enter through the endcaps. When the hohlraum is filled with gas, the polyimide stretches and bulges out to approximately 200 μm at the center of the hole along the hohlraum axis.

The targets are filled with gas to help create a medium that can be quickly and uniformly ionized by a frequency tripled Nd:glass laser, $3\omega_o = 0.35$ μm. The gas fill is chosen to provide an $n_e \leq 10^{21} cm^{-3}$ when it is fully ionized. At these densities, the laser energy is absorbed primarily by inverse bremsstralung. Unlike exploding foils where these densities are attained when the plasma has

expanded, here the laser heats the entire gas volume once the polyimide membrane has been quickly ablated . By choosing a gas density below n_{cr}, the bulk of the laser energy is not deposited at a critical density surface and this leads to a much larger and more uniform plasma than can be produced by exploding foils. The fill pressure is 1 atm for all gases and is monitored by a pressure transducer until the laser shot. For these studies, the typical gas was neopentane, C_5H_{12}, which produces a density of $10^{21}cm^{-3}$.

Different laser configurations were used to irradiate the two targets. In both cases, nine of the ten beams of Nova were used at a wavelength of 0.35 μm to heat the large volume of plasma to 3keV. The tenth beam was reserved for use as an interaction probe beam for the instability studies. For the gas bags, a square 1 ns pulse delivered ~ 2.5 kJ in each beam. For the gas-filled hohlraums, a 1.4 ns shaped pulse was used. It had a low intensity foot for the first 600 ps and then increased by a factor of 6.3 to a flat 800 ps plateau. The foot on the pulse was designed to ablate the window and heat the gas.

Initially in both target configurations, the laser beams must ablate the polyimide window that encloses the gas. Then the laser heats the gas by inverse bremsstrahlung and hydrodynamic calculations predict that approximately 60 % of the laser energy is absorbed by the gas. In the case of the gas bags, all ten beams pass through the center of the washer. Virtually the entire volume is irradiated by the overlapping laser beams, each of which is defocussed to produce a focal spot of 1.7 mm at the target midplane. For gas-filled hohlraums, the beams enter the hohlraum through the holes in the endcaps and the transmitted beams form elliptical focal spots that are approximately 600 μm x 950 μm on the inside Au wall. In the hohlraums, it is not possible to entirely heat the gas volume by the laser beams as in the gas bags. However, the laser energy not absorbed in the gas creates a radiation field inside the hohlraum; therefore

radiation transfer as well as electron conduction help to homogenize the temperature. The pathlength of the laser through the gas in both cases, the hohlraum and gas bag, is ~ 2.5 mm

PLASMA CHARACTERIZATION

Measuring the plasma parameters will enable us to validate theoretical models of the parametric instabilities. Therefore, characterization of these targets is extremely important to interpret the results obtained from these long scale-length plasmas. One advantage of these targets is that the gas fill determines the electron density. Furthermore, these targets require only ~ 300 J of energy to completely ionize the entire volume of gas. Thus, the electron temperature is the most important variable to measure since it directly affects the collisional absorption, the SRS filamentation, and the SBS threshold and growth rates.

X-ray imaging and x-ray spectroscopy are used to characterize the plasmas. The electron temperature was measured by using spectral line intensities arising from trace elements inserted into the plasmas on fibers or foils. The tracers provide spectral signals from pairs of elements that are analyzed for electron temperature by a collisional-radiative code.[4] We use mid-Z elements, Z = 17-24, as these are the most appropriate for producing *K*-shell diagnostics sensitive in 1 to 3 keV temperature plasmas. In the gas bags, fibers coated with 2000 Å of co-sputtered Ti and Cr were placed across the diameter of the washer. In addition, the gas was doped with 1% Ar and 1% Cl for further measurements of the temperature and uniformity. In the hohlraums, the tracer plasma was a 2000 Å deposit of Ti and Cr cosputtered onto a 800 Å thick CH foil substrate.

The technique for measuring the electron temperature is based on the ratio of line intensities of the same transition in two different elements. The isoelectronic

sequence technique, which has several advantages, is reported elsewhere.[5] The principle advantage of this technique is that the isoelectronic ratio is largely unaffected by the hydrodynamic evolution of the plasma. Because the two elements are close in Z, the ionization balance of the elements evolve in the same manner with temperature and density. Therefore, the resulting ratio is less time-dependent than the ratios formed between lines from different ion stages of the same element. For the gas bags, the He-like $1s^2$ ($^1S_0$)- 1s2p ($^1P_1$) transition, often called the He-like α line, and the 1s-2p Lyman α transition of titanium and chromium were used. Once the Ti/Cr coating is ablated, these lines are calculated to be optically thin by collisional-radiative codes. The measured Ti/Cr line ratio vs time from the gasbag targets is shown in Fig. 2 along with the predicted ratio for the case of a 1 ns heating pulse. In this data there is a delayed onset of the ratio due to the heating of the gas, however, after this point the ratio increases until the end of the heating pulse at 1 ns. The data indicate that the plasma temperature is between 2 to 3 keV and remains fairly constant. Line ratios involving the He-like and H-like line intensities from the Ar and Cl dopants were also obtained. These spectra are more appropriate for lower temperatures since the tracers become over-ionized above 2 keV . Analysis of these measurements are consistent with the Ti/Cr measurements and provide a lower bound on the T_e.[6]

In gas-filled hohlraums, the ratio of the $1s^2$ ($^1S_0$) - 1s3p ($^1P_1$), He-like β, of Ti and Cr is used. These lines are more optically thin than the $n = 2 - 1$ resonance lines and, for the conditions studied here, do not have underlying satellite lines that can affect the measurement. Because of the potential non-uniformity inside the hohlraum, the tracer is deposited in a 100 μm wide strip that is suspended in the hohlraum with the deposit facing the beam at the position shown in Fig 1. The experimental data, represented by circles in Fig. 3, show that the electron

temperature is ≥ 3 keV for a duration of ~ 500 ps. The ablation of the foil and the radiation temperature of the hohlraum were also investigated in related experiments. The full results and other experimental details of the measurements will be reported in a forthcoming publication.[7]

To provide an insight into the uniformity of the plasmas, gated x-ray pinhole images are used to provide two-dimensional snapshots of the plasma for photon energies > 2.5 keV. Typical images are shown in Fig. 4 at three different times during the heating of the gas bag. They were obtained by a time-resolved pinhole camera with 4x magnification and have a resolution of ~ 13 μm. Each image is integrated over ~ 100 ps. Areas of bright emission appear black in the images. In the first image, the emission from the bag is predominately from the polyimide membrane while in the two later time images, the emission is from the gas. The washer corresponds to a vertical white strip in the middle of the image because it obscures the emission from the gas in this line-of-sight. In the last image the apparent brightness increases at the edges of the washer because the emission of the gas is enhanced by emission from the glue and washer itself. The images show that after the initial ablation of the gas bag membrane, the gas heats very uniformly. More detailed results on the uniformity as well as the propagation have been discussed elsewhere. [8]

SBS IN LARGE HOMOGENEOUS PLASMAS

We now present an example of experiments that can be performed by a systematic variation of the targets. SBS and SRS instabilities are important because they can reduce the amount of laser energy absorbed by the plasma. The SBS instability results when an incident electromagnetic wave decays into an ion

acoustic wave and a scattered electromagnetic wave. If conditions are favorable, the incident and scattered wave can beat together and enhance the instability.

The magnitude of SBS or other instabilities can be estimated by solving the fluid equations for the propagation of electromagnetic waves in a plasma. By conservation of momentum and energy, dispersion relations can be derived. Furthermore, when the equations are linearized, threshold limits on SBS growth can be obtained. For particular assumptions, these wave relations can be solved to give different threshold limits. These thresholds represent the minimum conditions that must be present before the instability will grow. A standard criteria for SBS growth in a plasma with density and/or velocity gradients is when the instability increases by a factor of $e^{2\pi}$.

For comparison of these competing processes, threshold limits are usually discussed in terms of an inequality involving the term (v_{osc}/v_{therm}) where v_{osc} represents the velocity of the electrons oscillating in the electric field generated by the laser, and v_{therm} is the thermal velocity of the electrons in the plasma.

The simplest example of a threshold is the convective SBS damping threshold which is a necessary but not sufficient condition. It is given by:

$$\left[\frac{v_{osc}}{v_{therm}}\right]^2 \geq 4\left(\frac{\nu_{ei}}{\omega_o}\right)\frac{\nu_a}{\omega_{ia}}$$

where ν_{ei} is the collision frequency between the ions and electrons, ν_a is the energy damping rate of the ion acoustic wave, ω_o is the laser frequency, and ω_{ia} is the ion wave frequency. If this condition is not satisfied, then the damping is sufficient to breakup the instability.

However, if there is a small velocity scale-length in the plasma such as occurs in disks or exploding foils, then the wave matching condition necessary for *growth can not be supported unless:*

$$\left[\frac{v_{osc}}{v_{therm}}\right]^2 \geq \frac{16}{k_o L_v}\left(\frac{n_{cr}}{n_e}\right)$$

where the length L_V represents the velocity scale-length, and k_o is the wave number of the incident wave. Since, the velocity scale-length appears in the denominator, this condition is easier to satisfy for high temperature large scale-length plasmas than for exploding foil plasmas.

Therefore, for mm-size plasmas at high temperatures, another condition becomes important. In future ICF plasmas with long density and velocity scale-lengths, the relevant dispersion relation involves the finite length of the plasma. For homogeneous plasmas of finite length, L, the threshold is:

$$\left[\frac{v_{osc}}{v_{therm}}\right]^2 \geq 4\frac{\lambda_o}{L}\left(\frac{n_{cr}}{n_e}\right)\frac{v_a}{w_{ia}}$$

where λ_o is the wave length of the incident wave and L ~ 2 mm for these plasmas.

While the threhold equations are typically expressed in the above form involving the ion acoustic frequency, these equations can be recast in terms of fundamental plasma parameters: electron temperature and density. To examine

the sensitivity of the thresholds to the plasma conditions, the equations are expressed in terms of the probe beam intensity, I, as a function of electron temperature. The intensity subscripts are *d* for the convective damping, *vel* for the velocity gradient, and *L* for the homogeneous plasma of finite length.

$$I_d \propto \left(\frac{1}{T_e}\right)^{1/2}\left(\frac{n_e}{n_{cr}}\right)\left(\frac{1}{\lambda_o}\right)^3 \frac{\nu_a}{w_{ia}}$$

$$I_{vel} \propto T_e \left(\frac{n_{cr}}{n_e}\right)\left(\frac{1}{L_V\,\lambda_o}\right)$$

$$I_L \propto T_e \left(\frac{n_{cr}}{n_e}\right)\left(\frac{1}{L\,\lambda_o}\right)\frac{\nu_a}{w_{ia}}$$

the factor (ν_a/ω_{ia}) is approximately 0.2 for the plasmas primarily composed of carbon and hydrogen which we are investigating.

For the expected plasma lengths and scale-lengths in gas-filled targets of mm-size , Fig. 5 gives the threshold intensity of the probe beam as a function of electron temperature at a fixed density of 0.1 n_{cr}. The graph indicates that SBS can become important for laser intensities greater than $2 \times 10^{14} W/cm^2$ for electron temperatures of 3 keV.

Systematic variations of the target parameters have led to many interesting studies. These related series of experiments will be reported in upcoming papers that are in preparation. [9] Here we would like to limit the discussion to preliminary results of one set of experiments in which a small physical perturbation was introduced. The perturbation was created by a localized plasma resulting from the ablation of a 9 μm diameter carbon fiber in the path of the interaction probe beam. Figure 6 shows the SBS reflectivity both with and without a fiber for three different electron densities. Each gas fill corresponds to a different electron density. The abscissa in the graph shows the gas fills spaced roughly linearly with the decreasing density. As the gas density decreases, the addition of a fiber has a more pronounced effect on reducing the SBS. In the highest density gas, C_5H_{12}, the fiber and no fiber case have the same value; however, this value is near the limit of detection for the diagnostic. The data suggest that the addition of fibers in the target reduce the SBS reflectivity in gas bag targets.

Although these results are preliminary, they do demonstrate a trend that can be understood in terms of the scaling laws shown above. The addition of fibers may create localized perturbations in the density and plasma flow since the fiber continues to ablate during the pulse. While this is not a problem for the spectroscopy, it does reduce the velocity scale-lengths. Looking at Figure 5, it can be seen that a decrease of a factor of 5 in the velocity scale-length would increase the threshold above that predicted for a 2 mm long homogeneous, finite plasma. These results suggest that creating localized perturbations by adding fibers could be used to suppress SBS. Further experiments are needed to improve the statistics of these results, but they show that varying one parameter leads to a powerful way to verify analytical trends and gain insight into the physical processes.

SUMMARY AND CONCLUSIONS

Gas-filled targets were developed as a means of studying laser plasma interactions. The plasma conditions were chosen to mimic those expected in future ICF targets where large, homogeneous plasmas will be created inside of hohlraums. The results from experiments to characterize these plasmas demonstrate that the electron temperatures and electron densities obtained were ~ 3 keV and ~ 10^{21} cm^{-3}, respectively. Some preliminary SBS measurements are shown as an example to demonstrate how these large plasmas can be used as a testbed for systematic studies of physical processes. By changing the laser energy and gas fill, the plasma parameters can be easily varied. This versatility makes these targets a good candidates for other experiments that require a large uniform plasma.

***This work was performed under the auspices of the U.S. Department of Energy by Lawrence Livermore National Laboratory under contract No. W-7405-ENG-48.**

FIGURES

Figure 1. Schematic of gas bags and gas-filled hohlraums. The spectra for diagnosing electron temperature originate from the tracer materials shown in the diagrams. The gas-filled hohlraum shows two representative beams incident on the inside of the Au hohlraum with the gas-filled membrane bowing out from the endcaps. The gas bags are irradiated by 5 beams on each side that cross in the middle of the washer.

Figure 2. Electron temperature measurement of gas bags. The ratio of the Cr He-like α to the Ti He-like α predicted from a collisional-radiative code is shown for different electron temperatures. The data, shown by the squares, follow the calculated evolution of the target fairly well and agree best with the predictions of 2 to 3 keV. T = 0 corresponds to the start of the 1 ns square laser pulse.

Figure 3. Electron temperature measurement of gas-filled hohlraums. These measurements are taken from spectra from Ti/Cr tracer plasmas inside of the hohlraum target. The line intensity ratio of Cr He-like β to the Ti He-like β is shown. The results indicate that a plasma with $T_e > 3$ keV is created during the plateau of the shaped pulse.

Figure 4. X-ray images of a gas bag. The times are relative to a 1 ns square laser that begins at t = 0. Initially, the beams are visible on the polyimide membrane which confines the gas. The two later times show emission

> 2.5 keV that originates from the gas fill. The images indicate that the plasma is homogeneous.

Figure 5. Scaling laws for SBS for the interaction probe beam intensity as a function of electron temperature. The functional dependencies on electron temperature for the given scale-lengths discussed in the text are shown for three cases: damping, velocity gradient, and homogeneous finite plasma.

Figure 6. SBS reflectivity vs plasma gas. The x-axis is plotted as a function of the gas fill. The spacing along the abscissa is linear with the difference in electron density. Densities from left to right along the x-axis. The X symbol gives the results for targets with a fiber in the gas bag, while the squares are the results for targets with no fiber.

REFERENCES

[1] W. L. Kruer, *The Physics of Laser Plasma Interactions* (Addison-Wesley, Redwood City, CA, 1988); H. A. Baldis, E. M. Campbell, and W. L. Kruer, "Laser Plasma Interactions", in *Handbook of Plasma Physics*, Vol. 3: *Physics of Laser Plasma* , eds. A. M. Rubenchik and S. Witkowski (Elsevier Science Publishers B. V., 1991), pp. 361-434 and references therein.

[2] R. A. London and M. D. Rosen, Phys. Fluids **29**, 3813 (1986); R. P. Drake, R. E. Turner, B. F. Lasinski, E. A. Williams, D. W. Phillion, K. G. Estabrook, W. L. Kruer, E. M. Campbell, K. R. Manes, J. S. Hildum, and T. W. Johnston, Phys. Rev. Lett. **31**, 3130 (1988); R. P. Drake, E. A. Williams, P. E. Young, K. G. Estabrook, W. L. Kruer, and H. A. Baldis, Phys. Rev. Lett. **60**, 1018 (1988).

[3] L. V. Powers, et al., submitted to Phys. Rev. Lett.

[4] R. W. Lee, B. L. Whitten , and R. E. Strout, JQSRT **32**, 91 (1984).

[5] R. S. Marjoribanks, et al. Phys. Rev. A **46**, R3601 (1992); T. D. Shepard et al. ICF Quarterly Report **4**, (4), 137-144, LLNL UCRL - LR-105821-94-4 (1994); T. D. Shepard, et al. to be submitted to Phys. Rev. E.

[6] D. E. Klem, et al., Bull. Am. Phys. **39**, 1752 (1994); B. H. Failor, et al., Rev. Sci. Instrum. **66**, (1995).

[7] C. A. Back, et al. submitted to Phys. Rev. Lett.

[8] D. H. Kalantar, et al. ICF Quarterly Report **4**, (4), 145-151, LLNL UCRL - LR-105821-94-4 (1994); D. H. Kalantar, et al. accepted to Phys. of Fluids.

[9]B. J. MacGowan, et al, Bull. Am. Phys. **39**, 1662 (1994); D. S. Montgomery, et al., Bull. Am. Phys. **39**, 1752 (1994); B. J. MacGowan, et al. to be submitted to Phys. Rev. Lett.

SIDE VIEW OF HOHLRAUM

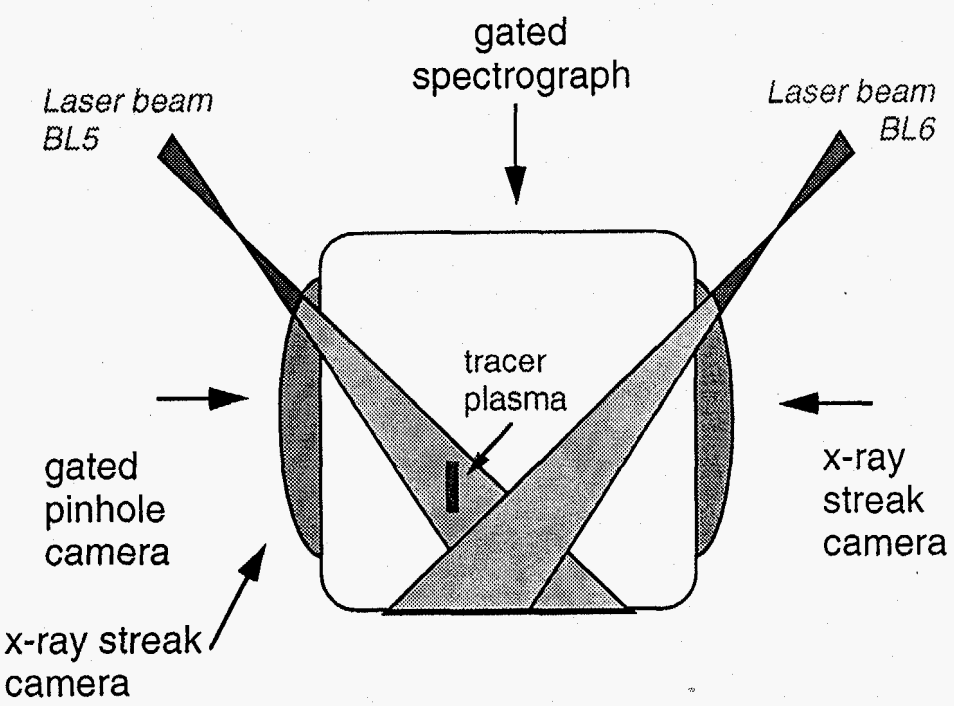

VIEW OF GAS BAG

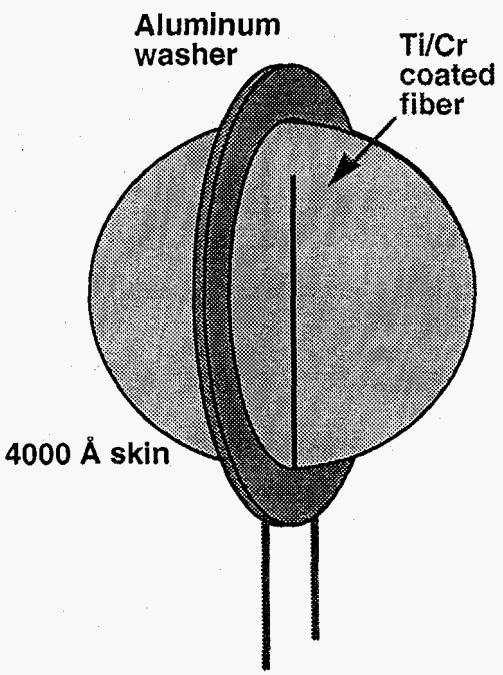

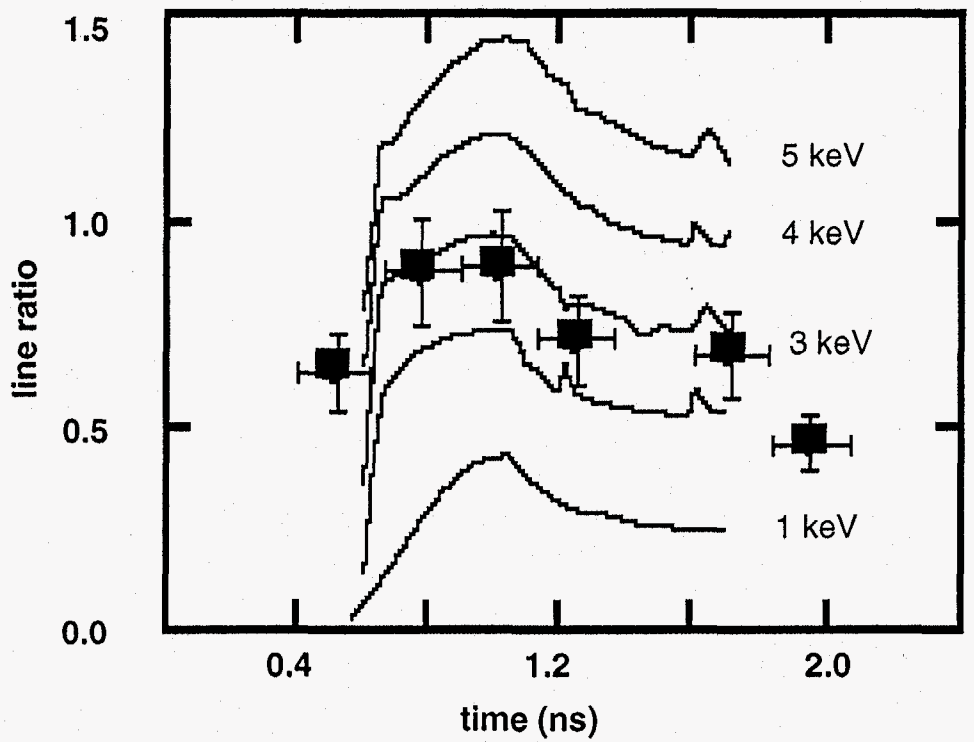
1.5
1.0
0.5
0.0
line ratio
5 keV
4 keV
3 keV
1 keV
0.4
1.2
2.0
time (ns)

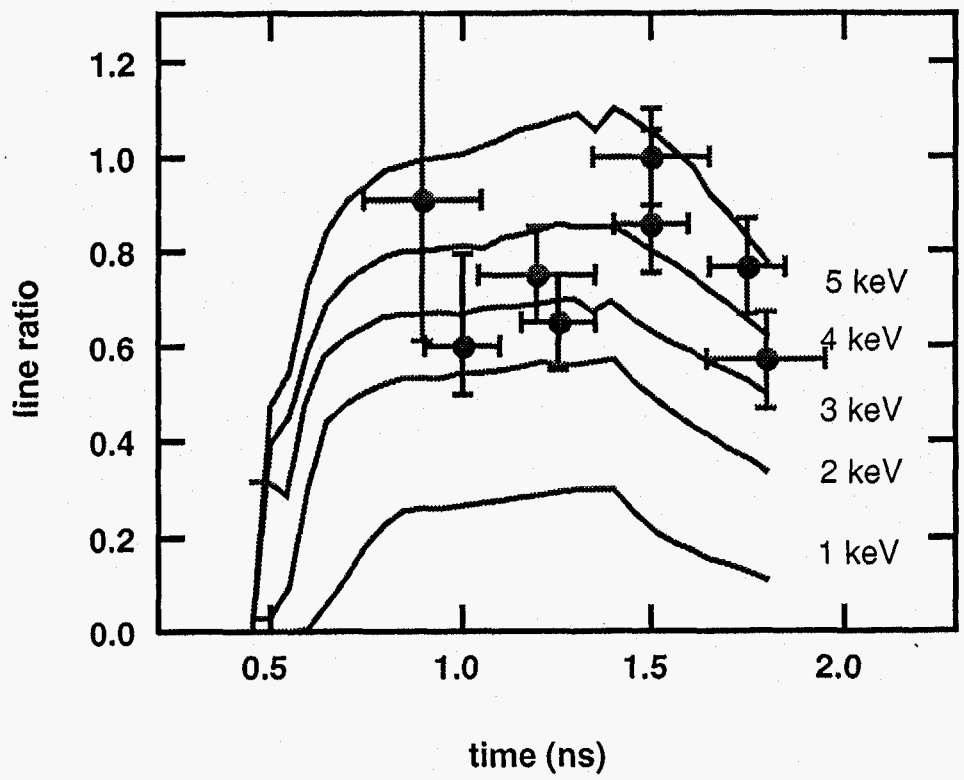
1.2
1.0
0.8
0.6
0.4
0.2
0.0
line ratio
0.5
1.0
1.5
2.0
time (ns)
5 keV
4 keV
3 keV
2 keV
1 keV

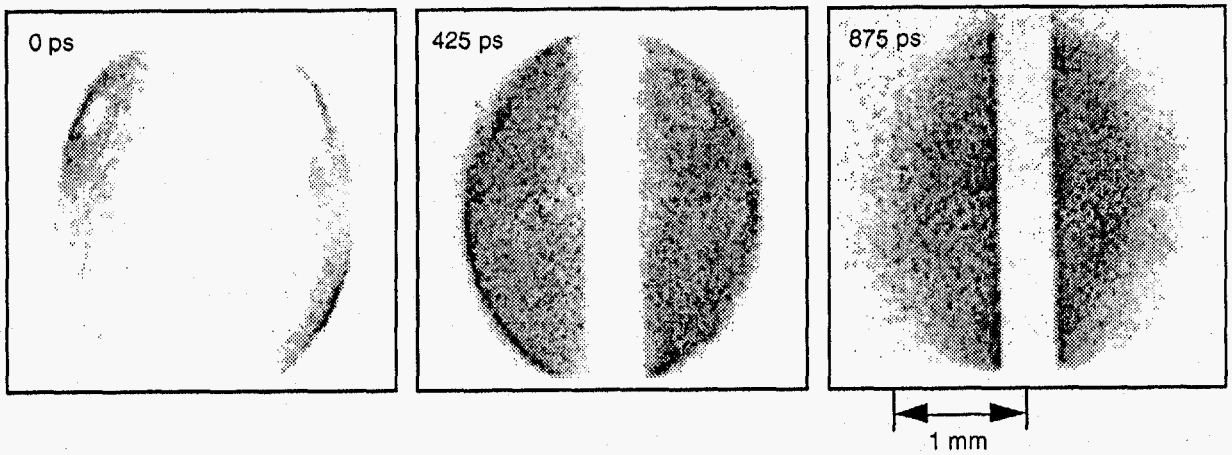
0 ps
425 ps
875 ps
1 mm

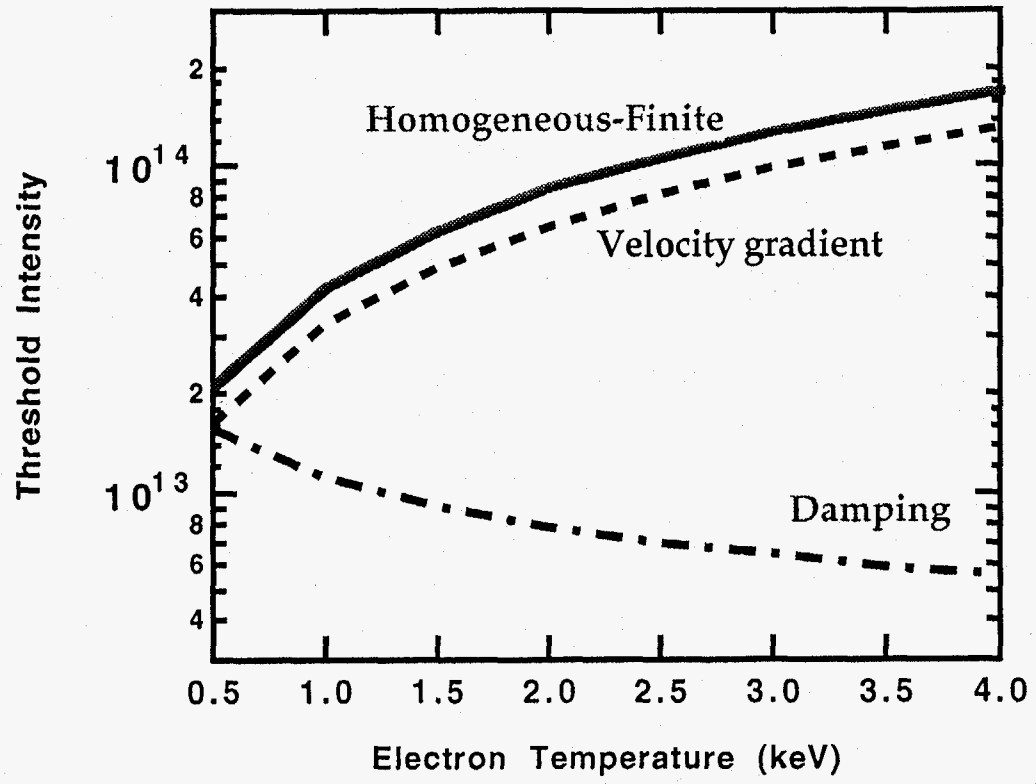
Threshold Intensity
10^{14}
10^{13}
2
8
6
4
2
8
6
4
Homogeneous-Finite
Velocity gradient
Damping
0.5
1.0
1.5
2.0
2.5
3.0
3.5
4.0
Electron Temperature (keV)

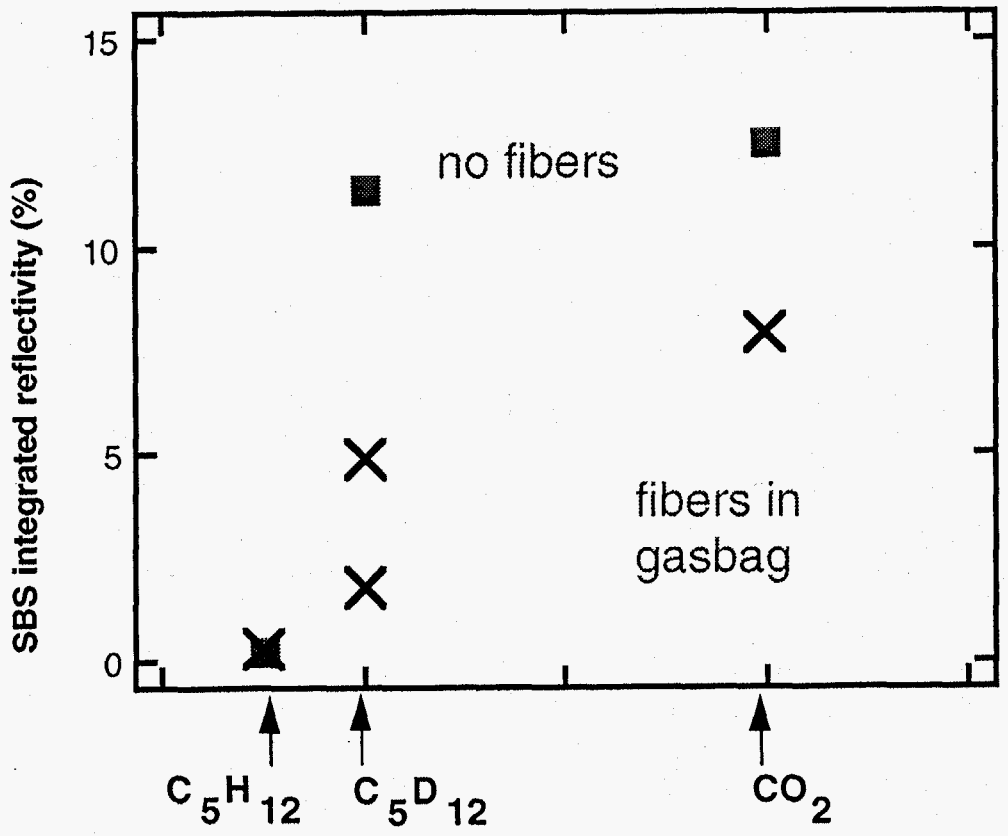
SBS integrated reflectivity (%)
15
10
5
0
no fibers
fibers in
gasbag
C_5H_{12}
C_5D_{12}
CO_2

Figure 1. C. A. Back, et al. submitted to JQSRT